



HAL
open science

Improved upper limits on the 21-cm signal power spectrum of neutral hydrogen at $z \approx 9.1$ from LOFAR

F.G. Mertens, M. Mevius, L.V.E Koopmans, A.R. Offringa, G. Mellema, S. Zaroubi, M.A. Brentjens, H. Gan, B.K. Gehlot, V.N. Pandey, et al.

► To cite this version:

F.G. Mertens, M. Mevius, L.V.E Koopmans, A.R. Offringa, G. Mellema, et al.. Improved upper limits on the 21-cm signal power spectrum of neutral hydrogen at $z \approx 9.1$ from LOFAR. Monthly Notices of the Royal Astronomical Society, 2020, 493 (2), pp.1662-1685. 10.1093/mnras/staa327 . hal-02504672

HAL Id: hal-02504672

<https://hal.science/hal-02504672>

Submitted on 24 May 2024

HAL is a multi-disciplinary open access archive for the deposit and dissemination of scientific research documents, whether they are published or not. The documents may come from teaching and research institutions in France or abroad, or from public or private research centers.

L'archive ouverte pluridisciplinaire **HAL**, est destinée au dépôt et à la diffusion de documents scientifiques de niveau recherche, publiés ou non, émanant des établissements d'enseignement et de recherche français ou étrangers, des laboratoires publics ou privés.

Cusp-to-core transition in low-mass dwarf galaxies induced by dynamical heating of cold dark matter by primordial black holes

Pierre Boldrini,¹★ Yohei Miki²,³ Alexander Y. Wagner,³ Roya Mohayaee,¹
Joseph Silk^{1,4,5} and Alexandre Arbey⁶

¹*Institut d'Astrophysique de Paris, UMR 7095, Sorbonne Université, CNRS, 98 bis Boulevard Arago, F-75014 Paris, France*

²*Information Technology Center, University of Tokyo, 5-1-5 Kashiwanoha, Chiba 277-8589, Japan*

³*Center for Computational Sciences, University of Tsukuba, 1-1-1 Tennodai, Tsukuba, Ibaraki 305-0006, Japan*

⁴*Department of Physics and Astronomy, The Johns Hopkins University, Baltimore, MD 21218, USA*

⁵*Beecroft Institute for Particle Astrophysics and Cosmology, Department of Physics, University of Oxford, Oxford OX1 3RH, UK*

⁶*Institut de Physique Nucléaire de Lyon, UMR 5822, Univ Lyon, Univ Lyon 1, CNRS/IN2P3, F-69622 Villeurbanne, France*

Accepted 2020 January 13. Received 2020 January 6; in original form 2019 May 31

ABSTRACT

We performed a series of high-resolution N -body simulations to examine whether dark matter candidates in the form of primordial black holes (PBHs) can solve the cusp–core problem in low-mass dwarf galaxies. If some fraction of the dark matter in low-mass dwarf galaxies consists of PBHs and the rest is cold dark matter, dynamical heating of the cold dark matter by the PBHs induces a cusp-to-core transition in the total dark matter profile. The mechanism works for PBHs in the 25–100 M_{\odot} mass window, consistent with the Laser Interferometer Gravitational-Wave Observatory (LIGO) detections, but requires a lower limit on the PBH mass fraction of 1 per cent of the total dwarf galaxy dark matter content. The cusp-to-core transition time-scale is between 1 and 8 Gyr. This time-scale is also a constant multiple of the relaxation time between cold dark matter particles and PBHs, which depends on the mass, the mass fraction, and the scale radius of the initial density profile of PBHs. We conclude that dark matter cores occur naturally in haloes composed of cold dark matter and PBHs, without the need to invoke baryonic processes.

Key words: galaxies: dwarf – galaxies: haloes – galaxies: kinematics and dynamics – galaxies: structure – dark matter.

1 INTRODUCTION

The nature of dark matter (DM) is one of the major unsolved problems in astrophysics. The most popular DM candidates include weakly interacting massive elementary particles (WIMPs), such as supersymmetric neutralinos or axions (Jungman, Kamionkowski & Griest 1996; Bergström 2000; Bertone, Hooper & Silk 2005). An alternative proposal to explain the nature of DM is that DM could be made of macroscopic compact halo objects (MACHOs) such as primordial black holes (PBHs; Zel'dovich & Novikov 1967; Hawking 1971; Khlopov 2010; Clesse & García-Bellido 2018). These PBHs could naturally be produced in the early Universe via cosmic inflation, without the need to appeal to new physics beyond the standard model (Clesse and García-Bellido 2015; Inomata et al. 2017). There are currently three allowed mass windows around 4×10^{-17} , 2×10^{-14} , and 25–100 M_{\odot} (Carr et al. 2017). PBHs can constitute much or even all of the

DM in these mass windows by considering only the most well-established bounds and neglecting those that depend on additional astrophysical assumptions. However, taking into account all of the astrophysical constraints means that the PBH+cold dark matter (CDM) fraction can still be as much as ~ 0.1 (Carr et al. 2017), and even larger in the lowest mass windows. Despite the fact that there is still no direct evidence for PBHs, the 25–100 M_{\odot} mass window is of special interest in view of the recent detection of black hole mergers by the Laser Interferometer Gravitational-Wave Observatory (LIGO; Abbott et al. 2016). Moreover, the observed LIGO detection rates can be explained for a PBH mass fraction of order 0.001–0.01 (Sasaki et al. 2016; Kovetz 2017). In the future, the *Laser Interferometer Space Antenna* (LISA) could potentially also detect PBHs in this mass window (Amaro-Seoane et al. 2017).

Although the CDM paradigm can successfully explain various observations at different scales, there are unresolved problems, most notably the cusp–core problem but also tensions with overpredictions of dwarf galaxy numbers and the too-big-to-fail and diversity issues (see e.g. Bullock & Boylan-Kolchin 2017 for a recent review). Here we focus on the core–cusp problem. Measurements of galaxy

* E-mail: boldrini@iap.fr

rotation curves and dynamical models of dwarf spheroidal galaxies (dSphs) have revealed that the density profile of the DM haloes is approximately constant at the centres of most dwarf galaxies and corresponds to a cored profile (Moore 1994; Burkert 1995; de Blok et al. 2001; Swaters et al. 2003; Spekkens, Giovanelli & Haynes 2005; Walker & Peñarrubia 2011). In contrast, cosmological simulations have generally predicted a steep power-law mass-density distribution at the centres of CDM haloes, specifically a cuspy profile (Fukushige & Makino 1997; Navarro, Frenk & White 1997; Moore et al. 1998; Navarro et al. 2010). One explanation for the cusp–core problem within the paradigm of CDM relies on the effect of baryonic physics in converting the cusp into a core via changes in the gravitational potential caused by stellar feedback redistributing gas clouds, generating bulk motions and galactic winds along with heating by dynamical friction of massive clumps (e.g. Navarro, Frenk & White 1996; El-Zant, Shlosman & Hoffman 2001; Goerdt et al. 2010; Inoue & Saitoh 2011; Ogiya & Mori 2011; Pontzen & Governato 2012; Teyssier et al. 2013).

In collisionless systems, stellar particle encounters lead to the relaxation of particles with similar kinetic energy and drive the system to energy equipartition. Systems composed of particles of differing masses will also drive mass segregation processes. As an example, massive stars or MACHOs fall towards the centre of the potential well and their energy is transferred to the lighter stars, which move away from the centre (Chandrasekhar 1943; Spitzer 1969). Consequently, the system can expand and the density profile of the system can change due to this diffusion process (Brandt 2016; Koushiappas & Loeb 2017; Zhu et al. 2018).

Here, in the numerical experiments, we explore the consequences of assuming the DM in galaxies consists of both CDM and PBHs. We propose that PBHs, as DM candidates, can induce a cusp-to-core transition in PBH+CDM haloes through gravitational heating from two principal mechanisms, dynamical friction by CDM particles on PBHs and two-body relaxation between PBH and CDM. We explore this transition using high performance N -body simulations on GPU to probe the PBH+CDM mass fraction f_m in $10^7 M_\odot$ dwarf galaxies. Our simulations allow a mass resolution of $1 M_\odot$ for DM particles. We work with PBHs in the 25–100 M_\odot mass window, which is consistent with the LIGO detections. The paper is organized as follows. Section 2 provides a description of N -body modelling and our numerical simulations. In Section 3, we show our simulation results and discuss the implications of PBH as a DM candidate. Section 4 presents our conclusions.

2 N-BODY MODELLING

In this work, we consider that a fraction of the DM consists of 25–100 M_\odot PBHs. Then, a DM halo is composed of CDM particles and PBHs (DM = PBH+CDM). We define the PBH+CDM mass fraction as

$$f_m = \frac{M_{\text{PBH}}}{M_{\text{CDM}}}, \quad (1)$$

where M_{PBH} and M_{CDM} are the total masses of PBHs and CDM particles. For our halo, we assume the Navarro–Frenk–White (NFW) form (Navarro et al. 1996)

$$\rho(r) = \rho_0 \left(\frac{r}{r_s}\right)^{-1} \left(1 + \frac{r}{r_s}\right)^{-2}, \quad (2)$$

with scale density ρ_0 and scale length r_s . The relaxation time is proportional to $N/\ln(N)$, where N is the number of particles. Assuming 100 M_\odot PBHs and $10^7 M_\odot$ halo, the particle relaxation

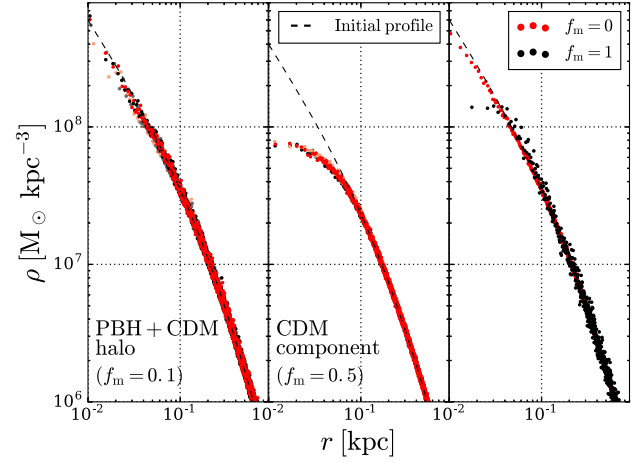


Figure 1. Tests of numerical accuracy. Density profiles of a halo composed of 100 M_\odot PBHs to test the impact of the accuracy control parameter A (left-hand panel) and softening length ϵ (middle panel) in simulations. We tested the impact of the accuracy control parameters of 2^{-6} (orange points), 2^{-7} (black points), 2^{-8} (grey points), and 2^{-9} (red points) for a halo with $f_m = 0.1$ and $r_s^{\text{PBH}} = r_s^{\text{CDM}}$. Density profiles of PBH+CDM halo (left-hand panel) hold the initial distribution for all the different parameter values. The middle panel shows our softening convergence test for the density profiles of the CDM component of $f_m = 0.5$ halo with a softening length $\epsilon = \epsilon_0/2$, ϵ_0 , and $2\epsilon_0$, where $\epsilon_0 = 1.331$ pc. Indeed, the core size of the CDM component is independent of the softening length. The right-hand panel describes density profiles of a halo composed only with CDM particles ($f_m = 0$) and a halo composed only with PBH particles ($f_m = 1$). The CDM profiles at the beginning $T = 0$ Gyr (dashed line) and at the end of the simulation $T = 11$ Gyr (red points), which are nearly identical, show the stability of our halo. However, there is core formation for $f_m = 1$ due only to two-body relaxation between PBHs.

will take between 1 and 12 Gyr depending on f_m considered between 1 and 0.01. In comparison, the relaxation time for 10^8 ($10^9 M_\odot$) haloes are 10 (100) times longer than for $10^7 M_\odot$ and longer than the age of the Universe, which is why we focus here on a $10^7 M_\odot$ dwarf galaxy, starting at redshift $z = 2$ in the simulations. Given the halo mass and redshift, the halo concentration c_{200} can be estimated from cosmological N -body simulations (Prada et al. 2012). Our halo is composed of DM and PBH particles with a total mass of $10^7 M_\odot$.

To generate our NFW haloes, we use the initial-condition generator, MAGI. Adoption of a distribution-function-based method ensures that the final realization of the halo is in dynamical equilibrium (Miki & Umemura 2018). We perform our simulations with the high performance collisionless N -body code, GOTHIC (Miki & Umemura 2017; Miki 2019). This gravitational OCTREE code runs entirely on GPU and is accelerated by the use of hierarchical time steps in which a group of particles has the same time step. We have performed the simulations using NVIDIA GeForce GTX 1080 Ti (CUDA 9.0) on Intel Xeon Silver 4114 (GCC 4.8). We evolve different PBH+CDM haloes composed of 25, 50, 75, and 100 M_\odot PBHs over 11 Gyr by adopting the softening length of $\epsilon_0 = 1.331$ pc and the accuracy control parameter of 2^{-7} . All runs were made with CDM particles of $1 M_\odot$. We explored also PBH+CDM haloes with different mass fractions $f_m = [0.01, 0.1, 0.5]$. In our simulations, we assume that the CDM and PBH components of PBH+CDM haloes initially follow NFW profiles with the same concentration. We tested two different scale lengths for the profile of the PBH component: $r_s^{\text{PBH}} = r_s^{\text{CDM}}$ and $r_s^{\text{PBH}} = r_s^{\text{CDM}}/2$. The second corresponds to a scenario where the density of PBHs is enhanced in the central region. Indeed,

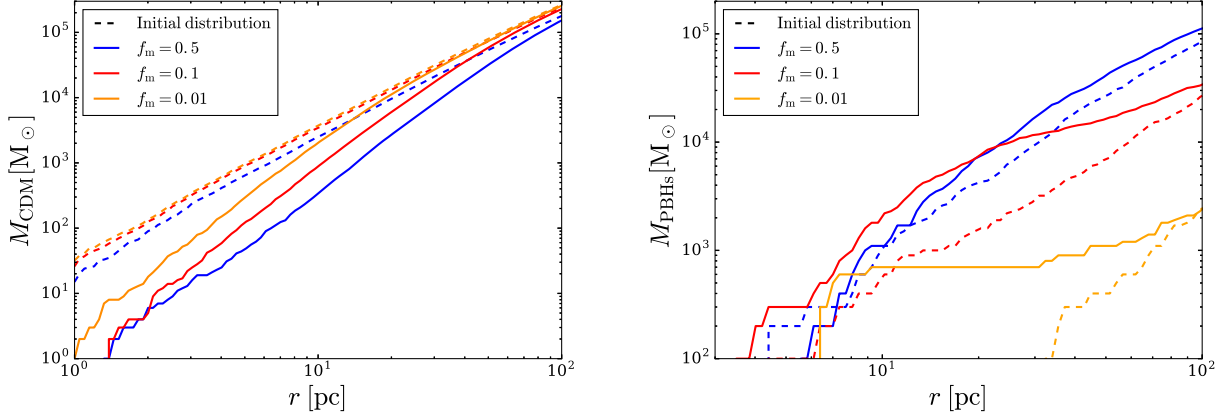


Figure 2. Autoredistribution of CDM particles and PBHs. Comparison between $T = 0$ Gyr (dashed line) and $T = 11$ Gyr (solid line) of the interior mass of the CDM component (left-hand panel) and $100 M_{\odot}$ PBHs (right-hand panel) as a function of radius for the three different mass fraction f_m and $r_s^{\text{PBH}} = r_s^{\text{CDM}}$. The profiles show that CDM particles moved to outer regions and PBHs felt to the halo centre. This phenomenon is due to dynamical friction by the CDM environment on PBHs and to a lesser extent by two-body relaxation between PBHs and CDM.

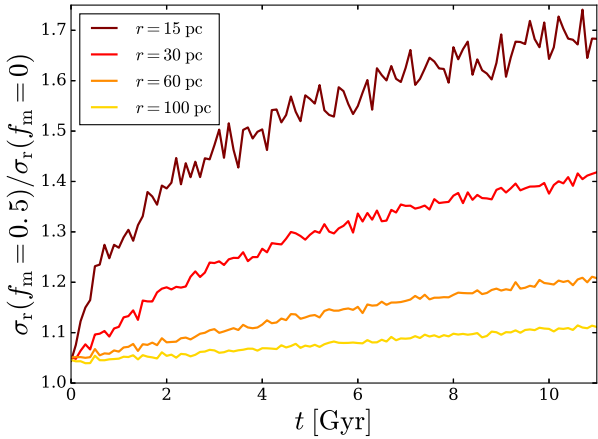


Figure 3. Heating of the CDM component. Ratio between CDM radial velocity dispersion for $f_m = 0.5$ and 0 haloes as a function of time at different radii. The PBH+CDM halo with $f_m = 0.5$ contains $100 M_{\odot}$ PBHs following an initial NFW profile with $r_s^{\text{PBH}} = r_s^{\text{CDM}}$. Over time, the velocity dispersion ratio increases, especially at the centre, due to PBH heating processes, which are two-body relaxation and dynamical friction effect of PBHs. This leads to core formation.

we suppose that mass segregation of PBHs would occur, and this increases the density of PBHs at the centre. This scenario should also enhance the formation of cores due to dynamical heating of the CDM by PBHs. It will also accelerate the two-body relaxation.

3 RESULTS

3.1 Evidences for core formation from gravitational heating by PBHs

First, we assess the impact on the PBH+CDM halo density profiles in our simulations of the two numerical parameters, which are the accuracy control parameter and the softening length ϵ . We tested 2^{-6} , 2^{-7} , 2^{-8} , and 2^{-9} for the accuracy control parameter in a PBH+CDM halo with $f_m = 0.1$ and $m_{\text{PBH}} = 100 M_{\odot}$. The left-hand panel of the Fig. 1 shows that PBH+CDM density profiles hold the initial distribution for all the different values of the accuracy control parameter. Additional accuracy tests confirmed also that the

density profile holds the initial distribution for the considered f_m and m_{PBH} values. To test how the softening length impacts on the density profile of the CDM component and the CDM core size, we ran simulations with three different softening lengths $\epsilon = \epsilon_0/2$, ϵ_0 , and $2\epsilon_0$ in order to ensure that our simulations do not suffer from numerical noise. We applied this test on a PBH+CDM halo with $f_m = 0.5$ and $m_{\text{PBH}} = 100 M_{\odot}$ expected to have core formation. The middle panel of Fig. 1 reveals that softening length (or particle size) does not affect the density profile of CDM component and its core size. Thus, numerical artefacts are not responsible for core formation. We tested also the stability of our halo composed only with CDM particles ($f_m = 0$) over 11 Gyr. We compare our halo profiles at the beginning ($T = 0$ Gyr) and at the end ($T = 11$ Gyr) of the simulation, which are nearly identical for all radii, on the right-hand panel of Fig. 1. We added the density profile of a halo composed only with PBHs ($f_m = 1$), which highlights core formation due to two-body relaxation between PBHs.

As we show that numerical effects do not initiate core formation, we need to provide evidence for the dynamical mechanism that will induce the cusp-to-core transition. Fig. 2 compares the interior mass of the CDM component (left-hand panel) and $100 M_{\odot}$ PBHs (right-hand panel) as a function of radius for three different mass fractions f_m between $T = 0$ and 11 Gyr. Profiles in Fig. 2 illustrate that contrary to the CDM particles, the number of PBHs increases in the central region. This results in the PBH infalling towards the central region. By falling in, PBHs will transfer energy to the CDM field via dynamical friction. This is the reason why CDM particles move to the outer regions as we see in the left-hand panel of Fig. 2. Another important dynamical effect is two-body relaxation between PBHs, which enhances the CDM particle migration. The CDM velocity dispersion is sensitive to these energy exchanges between CDM particles and PBHs. Fig. 3 compared the CDM radial velocity dispersion for $f_m = 0.5$ and 0 haloes as a function of time at different distances from the halo centre. The PBH+CDM halo with $f_m = 0.5$ contains $100 M_{\odot}$ PBHs following an initial NFW profile with $r_s^{\text{PBH}} = r_s^{\text{CDM}}$. We highlight that the velocity dispersion ratio increases rapidly, especially in the central region over time, due to PBH heating processes, which are two-body relaxation and dynamical friction effect of PBHs. This leads to core formation. In addition, Fig. 4 shows the evolution of the CDM density profiles and the CDM mass-weighted velocity distribution projected face-on through a 100 pc slice during a cusp-to-core transition for

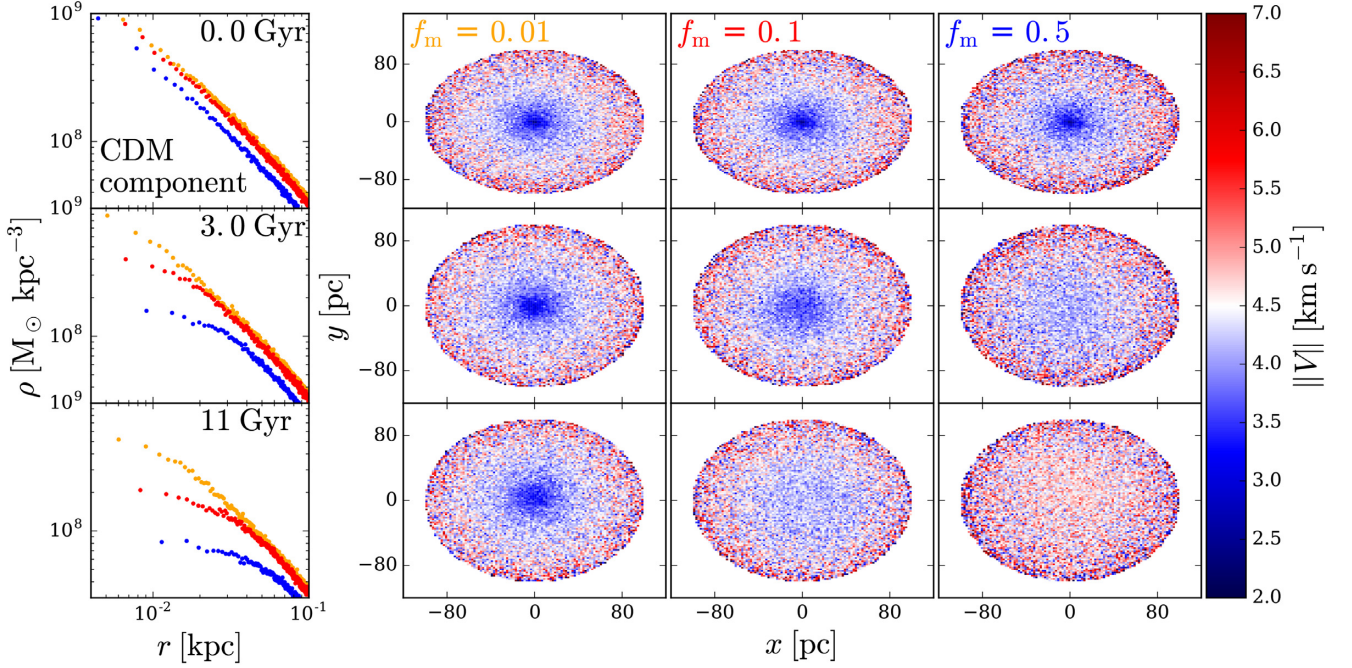


Figure 4. Cusp-to-core transition due to heating. Density profiles of the CDM component (left-hand panels) for $f_m = 0.01$ (yellow), 0.1 (red), and 0.5 (blue) with $100 M_\odot$ PBHs and $r_s^{\text{PBH}} = r_s^{\text{CDM}}$ and their corresponding maps of the CDM mass-weighted velocity distribution projected face-on through a 100 pc (right-hand panels) at $0, 3,$ and 11 Gyr . As the CDM velocity increases in the central region, the CDM density profile changes until core formation occurs. All the maps show that core formation goes with dynamical heating of DM particles.

the CDM component in a PBH+CDM halo with $f_m = 0.01, 0.1,$ and 0.5 by assuming $100 M_\odot$ PBHs and $r_s^{\text{PBH}} = r_s^{\text{CDM}}$. As the CDM velocity increases in the central region, the CDM density profile changes until core formation occurs. This figure demonstrates that core formation goes along with dynamical heating of CDM particles.

3.2 Core size and core formation time

Fig. 5 shows the overall density profiles of the PBH+CDM halo and the density profiles of the CDM and PBH components of the PBH+CDM halo separately after $T = 11 \text{ Gyr}$ for different initial mass fractions f_m , initial scale radii for the PBH component r_s^{PBH} , and initial PBH masses m_{PBH} . As we expect, two-body relaxation and dynamical friction effects from CDM particles modified all the density profiles. In order to determine if there is core formation in our haloes, we did a single-component fit for the PBH+CDM profile and separate fits for CDM and PBH profiles. We tested many profiles such as Einasto (Einasto 1965), Burkert (Burkert 1995), and Zavala (equation 4 in Zavala, Vogelsberger & Walker 2013) profiles. However, we found that all of our profiles are well fitted by the following five-parameter formula:

$$\rho(r) = \rho_c W(r) + (1 - W(r))\rho_{\text{NFW}}(r), \quad (3)$$

where ρ_c is the central core density and $W(r)$ is defined as

$$2W(r) = 1 - \text{erf}\left(\frac{r - r_c}{2\Delta}\right), \quad (4)$$

where r_c is the core radius and Δ is a parameter to control the sharpness of the transition from the core to the NFW profile. The error function corresponds to a switching function here. Our fitting formula reproduces the simulated density structures and captures the rapid transition from the cusp to the core. We set Poissonian

errors for fitting weights. Our results suggest that it is natural to have multiple cores for a two-component halo. Indeed, the core radii of the PBH+CDM halo, the CDM component, and the PBH component differ. Based on a reduced chi-squared method, fits of the CDM component of the PBH+CDM halo provide the best-fitting values of core radii (see Table 1). We consider these core radii to determine whether a transition appears in our simulation. The smallest core size in the simulations is of the order of 10 pc , which corresponds to our spatial resolution. Thus, we assume that a cusp-to-core transition occurred when the core size r_c becomes greater than our spatial resolution. Table 1 describes the best-fitting values for core sizes for the CDM component of the PBH+CDM halo for all our simulation scenarios. In the case where the density of PBHs is enhanced in the central region ($r_s^{\text{PBH}} = r_s^{\text{CDM}}/2$), the dynamical heating by PBHs generates larger core sizes (see also Fig. 5).

Now, we have the relation between the core radius $r_c(t)$ of the CDM component of the PBH+CDM halo and the time t when the cusp-to-core transition occurs in the simulations. We invert this function in order to calculate the time ratio $T_c(r_c)/T_r(r_c)$, where $T_c(r_c)$ and $T_r(r_c)$ are the core formation time and the relaxation time, respectively. The relaxation time T_r is given by (Binney & Tremaine 2008)

$$T_r(r) \simeq \frac{v^3(r)}{8\pi(n_{\text{CDM}}m_{\text{CDM}}^2 + n_{\text{PBH}}m_{\text{PBH}}^2)G^2 \ln\left(\frac{r_{200}}{\epsilon}\right)}, \quad (5)$$

where n_{CDM} and m_{CDM} (n_{PBH} and m_{PBH}) are the number density and mass of CDM (PBH) particles, respectively. v , ϵ , and r_{200} represent the velocity, the softening length, and the virial radius, respectively.

Fig. 6 illustrates the time ratio $T_c(r_c)/T_r(r_c)$ as function of the core formation time $T_r(r_c)$ for all the simulation runs where a cusp-to-core transition occurred (see Table 1). We notice that the ratio

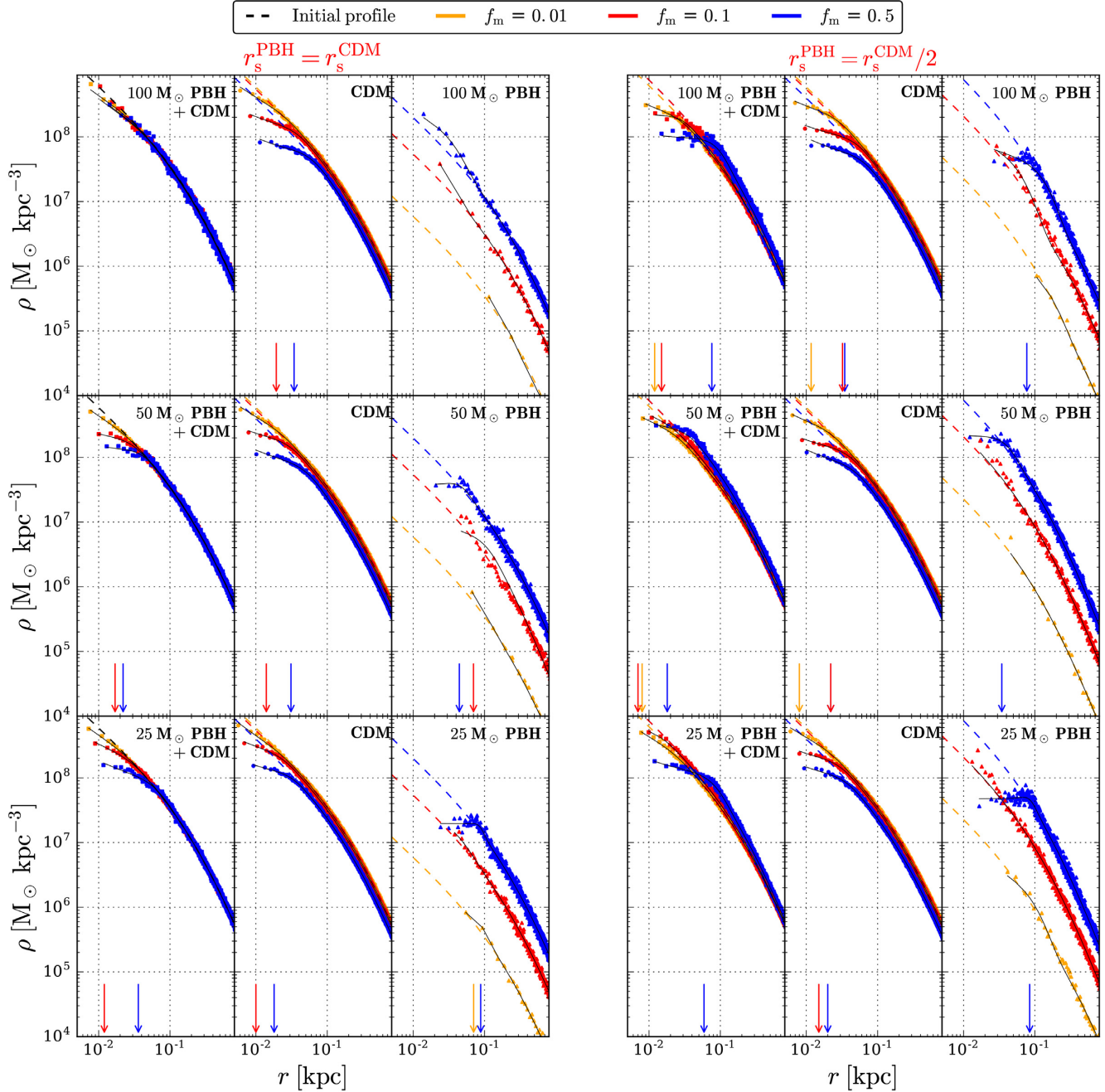


Figure 5. Cusp-to-core transitions in PBH+CDM haloes. In each subset, the left-hand panel corresponds to the overall density profiles of the PBH+CDM halo, the middle and right-hand panels to the density profiles of the CDM and PBH components of the PBH+CDM halo separately after $T = 11$ Gyr. Initially, the PBH and CDM components of the PBH+CDM halo with a total mass of $10^7 M_\odot$ follow NFW density profiles (dashed lines). We tested two different scale lengths for the profile of the PBH component: $r_s^{\text{PBH}} = r_s^{\text{CDM}}$ (left-hand column) and $r_s^{\text{PBH}} = r_s^{\text{CDM}}/2$ (right-hand column). We explore three different PBH+CDM mass fractions $f_m = [0.01, 0.1, 0.5]$ (see equation 1). Heating processes between PBH and CDM particles induce a transition from cusp to core in a PBH+CDM halo. In order to determine if there is this transition in our PBH+CDM halo, we did fit (black lines) for the three different density profiles and the size of formed cores is marked by arrows. Our results suggest that it is natural to have multiple cores for a two-component halo. Indeed, the core radii of the PBH+CDM halo, the CDM component, and the PBH component differ. In the case where the density of PBHs is enhanced in the central region ($r_s^{\text{PBH}} = r_s^{\text{CDM}}/2$), the dynamical heating by PBHs generates larger core sizes (see also Table 1).

$T_c(r_c)/T_r(r_c)$ is almost constant over the time in most of simulation runs. Furthermore, it does not strongly depend on the fraction f_m , the PBH mass m_{PBH} , or the PBH scale radius r_s^{PBH} . We derive that a cusp-to-core transition occurred for $T_c(r)/T_r(r) \lesssim 300$. The discrepancy between the time ratio values is certainly due to our core estimation based only on the CDM component.

Fig. 7 represents core size and core formation time maps in (f_m, m_{PBH}) space for both r_s^{CDM} and $r_s^{\text{CDM}}/2$ models. The core radii were calculated for $T_c = 11$ Gyr. In order to draw these maps, we predict r_c and T_c by setting the time ratio $T_c(r_c)/T_r(r_c)$ at 300 and calculating the relaxation time (see equation 5). Indeed, the white line in top panels of Fig. 7, which marks the limit of the cusp-to-core

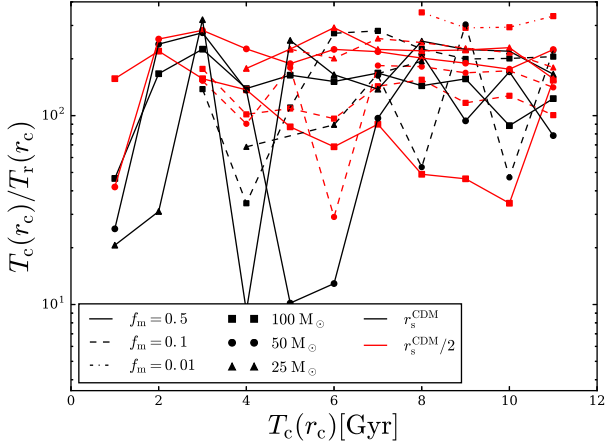


Figure 6. Estimating core formation time. Ratio between the core formation time $T_c(r_c)$ and the relaxation time $T_r(r_c)$ as a function of the core formation time $T_c(r_c)$ for all the simulation scenarios where a cusp-to-core transition occurred (see Table 1). This ratio is almost constant over the time in most of simulation scenarios and does not strongly depend on the fraction f_m , the PBH mass m_{PBH} , or the PBH scale radius r_s^{PBH} . Indeed, we establish that the time ratio is $\mathcal{O}(100)$ for both scale radii of the PBH component r_s^{PBH} .

Table 1. Best-fitting values for core sizes for the CDM component of the PBH+CDM halo with their corresponding reduced chi-squared χ^2/ν for all our simulation scenarios. From left to right, the columns give: the PBH–CDM mass fraction; the scale length for the PBH component; the PBH mass; if or no cusp-to-core transition (CCT) occurs; the core radius of the CDM component; and the reduced chi-squared. All these cores are resolved in simulations based on our resolution of about 10 pc when a CCT occurs. In the case where the density of PBHs is enhanced in the central region ($r_s^{\text{PBH}} = r_s^{\text{CDM}}/2$), the dynamical heating by PBHs generates larger core sizes (see Fig. 5).

f_m	$r_s^{\text{PBH}}/r_s^{\text{CDM}}$	m_{PBH} (M_\odot)	CCT	r_c (pc)	χ^2/ν
0.5	1	25	✓	17.6	1.01
0.5	1	50	✓	31.28	1.02
0.5	1	100	✓	34.32	1.0
0.1	1	25	✓	10.01	1.01
0.1	1	50	✓	14.48	1.0
0.1	1	100	✓	19.33	1.03
0.01	1	25	×	–	–
0.01	1	50	×	–	–
0.01	1	100	×	–	–
0.5	1/2	25	✓	19.7	1.05
0.5	1/2	50	✓	22.48	0.99
0.5	1/2	100	✓	34.63	1.06
0.1	1/2	25	✓	15.1	1.02
0.1	1/2	50	✓	21.55	1.02
0.1	1/2	100	✓	32.23	1.01
0.01	1/2	25	×	–	–
0.01	1/2	50	×	–	–
0.01	1/2	100	✓	11.73	0.99

transition, is consistent with the shape of the CDM distribution from simulations (triangles and squares) under this latter assumption. As one can see, core radius maps in Fig. 7 demonstrate that higher PBH mass and mass fraction in PBH+CDM halo generates larger core sizes. Enhancing the density of PBHs in the central region ($r_s^{\text{PBH}} = r_s^{\text{CDM}}/2$) lowers the threshold of the cusp-to-core transition (white line). Moreover, our maps show that at least a mass fraction of

1 per cent is needed to induce cores in PBH+CDM halo depending on the PBH mass and r_s^{PBH} . The core formation time was calculated at $r_c = 10$ pc because we assume that a cusp-to-core transition occurred when the core size r_c becomes greater than our spatial resolution of about 10 pc. These maps (see bottom panels in Fig. 7) reveal that the cusp-to-core transition takes between 1 and 8 Gyr to occur depending on the fraction f_m , the PBH mass m_{PBH} , and the PBH scale radius r_s^{PBH} . Enhancing the density of PBHs in the central region accelerates the formation of cores.

We highlighted that the dynamical heating of the CDM component by PBHs can induce cusp-to-core transitions without the presence of baryons and happens automatically in all PBH+CDM haloes. Experimentally, annihilation rates from pure CDM haloes can prove or or disprove this scenario quite clearly (Diemand, Moore & Stadel 2005; Ishiyama, Makino & Ebisuzaki 2010). A baryonic feedback scenario requires starbursts that occur at a particular resonance frequency for a given galaxy potential (Ogiya & Mori 2011). A single event blowout results in a temporary core that quickly reverts back to a cusp. This mechanism shown in this work can work even in such failed cases. In addition, low-mass galaxies, such as our PBH+CDM haloes, can merge after the cusp-to-core transition in order to form more massive galaxies ($10^8 M_\odot$) with a larger halo cores, which are consistent with observed galaxies. In fact, only a merger of two cored haloes yields a cored halo, because a merger of a cuspy halo with a cored halo or a second cuspy halo produces cuspy halo (Boylan-Kolchin & Ma 2004).

4 CONCLUSIONS

In this paper, we address one of the unresolved problem at small scales, the cusp–core problem, in $10^7 M_\odot$ haloes such as low-mass dwarf galaxies by considering the possibility that a fraction of the DM is made of PBHs. We show that the dynamical heating of the CDM component through PBH infall and two-body relaxation between PBHs induce the formation of cores in PBH+CDM haloes. We ran N -body simulations with a high performance and fully GPU-adapted code in order to provide strong evidence for these dynamical heating processes responsible for core formation. We confirm that PBHs as DM candidates can initiate a cusp-to-core transition in these low-mass galaxies. Our results suggest also that it is natural to have multiple cores for a two-component halo. Then, we test the PBH+CDM mass fraction f_m and PBH mass m_{PBH} . We work with PBHs in the 25–100 M_\odot mass window, which is consistent with the LIGO detections. Our simulations allow a mass resolution of 1 M_\odot for CDM particles. Finally, we derive a criterion based on the relaxation time in order to determine if a cusp-to-core transition occurred: $T_c(r)/T_r(r) \leq 300$. Based on our criterion, we set the lower limit on the PBH+CDM mass fraction to be 1 per cent of the total DM content to induce cores in PBH+CDM halo depending on the PBH mass and r_s^{PBH} . Here, we have shown that this scenario works even for a small fraction of PBHs. We determine that the cusp-to-core transition takes between 1 and 8 Gyr to appear, depending on the fraction f_m , the PBH mass m_{PBH} , and the PBH scale radius r_s^{PBH} . After a transition, the major impact of the PBH+CDM mass fraction and PBH mass is on the core size. Indeed, a larger PBH fraction and PBH mass will induce a larger core radius. As cores occur naturally in PBH+CDM haloes without the presence of baryons, there is no cusp–core problem in this alternative theory. As low-mass galaxies require less than 8 Gyr to form cores, higher mass galaxies with larger cores as observed can form in the hierarchical scenario. The existence of PBHs in the mass range studied here, 25–100 M_\odot , can possibly be confirmed by the *LISA* mission.

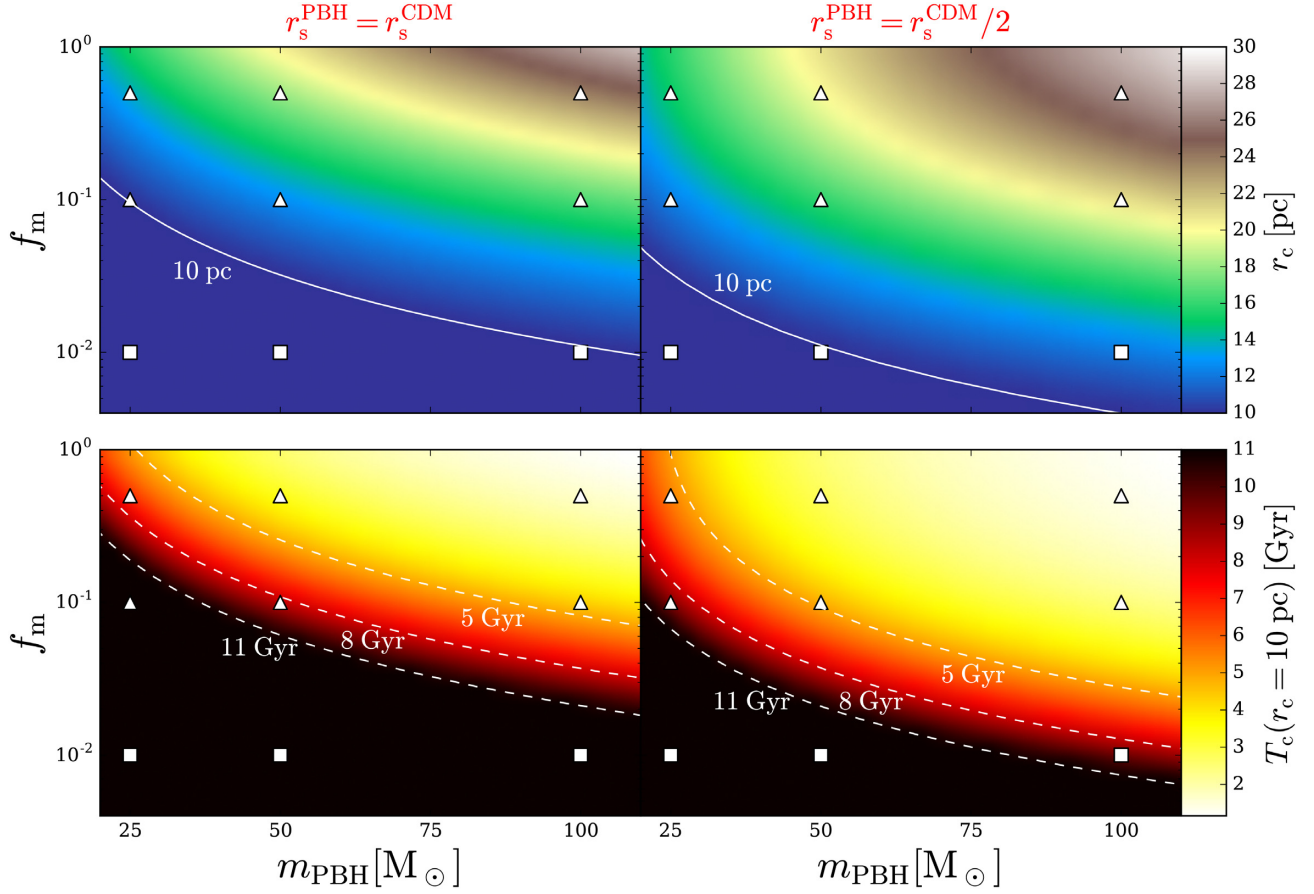


Figure 7. Core size and core formation time. Core size (top panels) and core formation time (bottom panels) maps in (f_m, m_{PBH}) space for both r_s^{CDM} and $r_s^{\text{CDM}}/2$ models. The core radii were calculated for $T_c = 11$ Gyr. Triangles (squares) on maps specify that a PBH+CDM halo for a given f_m and m_{PBH} has a cored (cuspy) profile based on our simulation results. The white line in top panels, which marks the limit of the cusp-to-core transition, is consistent with the shape of the CDM distribution from the simulations (triangles and squares) under this latter assumption. Core radius maps demonstrate that higher PBH mass and mass fraction in PBH+CDM halo generate larger core sizes. Enhancing the density of PBHs in the central region ($r_s^{\text{PBH}} = r_s^{\text{CDM}}/2$) lowers the threshold of the cusp-to-core transition (white line). At least a mass fraction of 1 per cent is needed to induce cores in PBH+CDM haloes depending on the PBH mass and r_s^{PBH} . The core formation time maps (bottom panels) reveal that the cusp-to-core transition takes between 1 and 8 Gyr to occur depending on the fraction f_m , the PBH mass m_{PBH} , and the PBH scale radius r_s^{PBH} . The core formation time was calculated at $r_c = 10$ pc because we assume that a cusp-to-core transition occurred when the core size r_c becomes greater than our spatial resolution of about 10 pc. Enhancing the density of PBHs in the central region accelerates the formation of cores.

ACKNOWLEDGEMENTS

We thank the anonymous referee for helpful comments and suggestions that improved our work. We would like to thank Dante Von Einzbern, Apolline Guillot, and Georges Boole for their constructive suggestions to improve the manuscript. YM is supported by ‘Joint Usage/Research Center for Interdisciplinary Large-scale Information Infrastructures’ and ‘High Performance Computing Infrastructure’ in Japan (Project ID: jh180045-NAH, jh190057-NA).

REFERENCES

Abbott B. P. et al., 2016, *Phys. Rev. Lett.*, 116, 061102
Amaro-Seoane P. et al., 2017, preprint (arXiv:1702.00786)
Bergström L., 2000, *Rep. Progress Phys.*, 63, 793
Bertone G., Hooper D., Silk J., 2005, *Phys. Rep.*, 405, 279
Binney J., Tremaine S., 2008, *Galactic Dynamics*, 2nd edn. Princeton Univ. Press, Princeton, NJ
Boylan-Kolchin M., Ma C.-P., 2004, *MNRAS*, 349, 1117
Brandt T. D., 2016, *ApJ*, 824, L31

Bullock J. S., Boylan-Kolchin M., 2017, *ARA&A*, 55, 343
Burkert A., 1995, *ApJ*, 447, L25
Carr B., Raidal M., Tenkanen T., Vaskonen V., Veermäe H., 2017, *Phys. Rev. D*, 96, 023514
Chandrasekhar S., 1943, *Rev. Modern Phys.*, 15, 1
Clesse S., García-Bellido J., 2015, *Phys. Rev. D*, 92, 023524
Clesse S., García-Bellido J., 2018, *Phys. Dark Universe*, 22, 137
de Blok W. J. G., McGaugh S. S., Bosma A., Rubin V. C., 2001, *ApJ*, 552, L23
Diemand J., Moore B., Stadel J., 2005, *Nature*, 433, 389
Einasto J., 1965, *Trudy Astrofizicheskogo Inst. Alma-Ata*, 5, 87
El-Zant A., Shlosman I., Hoffman Y., 2001, *ApJ*, 560, 636
Fukushige T., Makino J., 1997, *ApJ*, 477, L9
Goerdt T., Moore B., Read J. I., Stadel J., 2010, *ApJ*, 725, 1707
Hawking S., 1971, *MNRAS*, 152, 75
Inomata K., Kawasaki M., Mukaida K., Tada Y., Yanagida T. T., 2017, *Phys. Rev. D*, 96, 43504
Inoue S., Saitoh T. R., 2011, *MNRAS*, 418, 2527
Ishiyama T., Makino J., Ebisuzaki T., 2010, *ApJ*, 723, L195
Jungman G., Kamionkowski M., Griest K., 1996, *Phys. Rep.*, 267, 195
Khlopov M. Y., 2010, *Res. Astron. Astrophys.*, 10, 495
Koushiappas S. M., Loeb A., 2017, *Phys. Rev. Lett.*, 119, 041102

- Kovetz E. D., 2017, *Phys. Rev. Lett.*, 119, 131301
- Miki Y., 2019, in *ICPP 2019: Proceedings of the 48th International Conference on Parallel Processing*. ACM, New York, p. 1
- Miki Y., Umemura M., 2017, *New Astron.*, 52, 65
- Miki Y., Umemura M., 2018, *MNRAS*, 475, 2269
- Moore B., 1994, *Nature*, 370, 629
- Moore B., Governato F., Quinn T., Stadel J., Lake G., 1998, *ApJ*, 499, L5
- Navarro J. F., Frenk C. S., White S. D. M., 1996, *ApJ*, 462, 563
- Navarro J. F., Frenk C. S., White S. D. M., 1997, *ApJ*, 490, 493
- Navarro J. F. et al., 2010, *MNRAS*, 402, 21
- Ogiya G., Mori M., 2011, *ApJ*, 736, L2
- Pontzen A., Governato F., 2012, *MNRAS*, 421, 3464
- Prada F., Klypin A. A., Cuesta A. J., Betancort-Rijo J. E., Primack J., 2012, *MNRAS*, 423, 3018
- Sasaki M., Suyama T., Tanaka T., Yokoyama S., 2016, *Phys. Rev. Lett.*, 117, 61101
- Spekkens K., Giovanelli R., Haynes M. P., 2005, *AJ*, 129, 2119
- Spitzer L., 1969, *ApJ*, 158, L139
- Swaters R. A., Madore B. F., van den Bosch F. C., Balcells M., 2003, *ApJ*, 583, 732
- Teyssier R., Pontzen A., Dubois Y., Read J. I., 2013, *MNRAS*, 429, 3068
- Walker M. G., Peñarrubia J., 2011, *ApJ*, 742, 20
- Zavala J., Vogelsberger M., Walker M. G., 2013, *MNRAS*, 431, L20
- Zel'dovich Y. B., Novikov I. D., 1967, *SvA*, 10, 602
- Zhu Q., Vasiliev E., Li Y., Jing Y., 2018, *MNRAS*, 476, 2

This paper has been typeset from a $\text{\TeX}/\text{\LaTeX}$ file prepared by the author.